

SLOVAK UNIVERSITY OF TECHNOLOGY IN BRATISLAVA
Faculty of Electrical Engineering and Information Technology

Reg. No.: FEI-104400-99130



Superconducting flux pumps for motors, generators and magnets

Summary of doctoral dissertation

MSc. Asef Ghabeli Juybari

Study programme: Physical Engineering

Study field: Electrical and Electronics Engineering

Training workplace: Institute of Electrical Engineering
Slovak Academy of Sciences

Supervisor: Mgr. Enric Pardo, PhD

Bratislava 2021

This thesis was developed in a full-time doctoral study at Institute of Electrical Engineering, Slovak Academy of Sciences, Department of Superconductors, in Bratislava.

Author: **MSc. Asef Ghabeli Juybari**
Institute of Electrical Engineering SAS
Dúbravská cesta 9,
841 04 Bratislava

Supervisor: **Mgr. Enric Pardo, PhD**
Institute of Electrical Engineering SAS
Dúbravská cesta 9,
841 04 Bratislava

Opponents: **doc. RNDr. Tomáš Plecenik, PhD.**
Comenius University in Bratislava
Mlynská dolina,
842 48 Bratislava

Dr. Min Zhang
University of Strathclyde
204 George Street, Glasgow, G11XW,
United Kingdom

Dissertation thesis abstract was sent:

Dissertation Thesis defence will be held on:

Dean of the faculty FEI, STU: prof. Dr. Ing. Miloš Oravec

Contents

- 1 Summary** **1**

- 2 Calculation methods** **3**
 - 2.1 MEMEP 3D method 3
 - 2.1.1 Mesh definition 4
 - 2.2 MEMEP 2D method 5
 - 2.2.1 Mesh definition 6
 - 2.3 HTS tape resistivity 6
 - 2.4 Analytical method for coil charging 7

- 3 General Definitions** **7**

- 4 Open-circuit case results** **9**
 - 4.1 Main behavior of HTS dynamo 9
 - 4.2 Effect of tape critical current 10
 - 4.3 Airgap dependence of open-circuit voltage 10
 - 4.4 Impact of Magnet Geometry on Open-Circuit Voltage 12

- 5 Coil charging case results** **13**
 - 5.1 *I-V* Curve 14
 - 5.2 Instantaneous current 15
 - 5.3 Charging Behavior 15

- 6 3D modeling case results** **16**
 - 6.1 Current and Electric Field Analysis 16
 - 6.2 Impact of Tape Length on Voltage Generation 17
 - 6.3 Comparison to Experiments 19

- 7 Conclusions** **22**

1. Summary

The discovery of high-temperature superconductors (HTS), being able to operate at temperatures near the boiling of liquid nitrogen (77 K), changed the perspective of practical utilization of superconductivity in industry. Afterward, progress in the manufacturing technology of HTS REBCO coated conductors, paved the way for employing HTS coated conductors in magnets and power electric devices such as motors, generators, and fault current limiters.

HTS flux pumps are promising devices to maintain steady current mode in HTS magnets or to energize rotor windings in motors and generators in a contactless way. Among different types of flux pumps, the dynamo-type flux pump has become common due to its simple structure and ease of maintenance. However, understanding the principle of dynamo-type flux pump and revealing the details regarding the process of voltage generation and charging a coil connected to the flux pump have been challenging despite the recent progress.

In this thesis, we present 2D and 3D modeling methods based on minimum electromagnetic entropy production (MEMEP) method for analyzing the performance of a dynamo-type flux pump in open-circuit mode and charging a coil. Our presented models are efficient and fast compared to conventional commercial finite-element methods since they solve the Maxwell equations only inside the superconducting region with minimization of a functional and avoid rotating mesh in the air.

In 2D and open-circuit mode, by analyzing the DC open-circuit voltage in a high airgap range, we find that the DC voltage generation does not cease even in large airgaps. We also realize that the open-circuit voltage, with assuming constant J_c , does not depend on the J_c value, as long as the tape is fully saturated by screening currents. By changing the magnet size with equal width and height, it is revealed that it is not necessary to have magnets narrower than the tape in order to achieve flux pumping. To verify the modeling results, we compare them with measurements for several airgaps from [1] showing good agreement.

The MEMEP 2D method is further developed to investigate the charging process of a coil by an HTS dynamo. For the process of charging, our method is compared with the segregated \mathbf{H} -formulation finite-element method (calculated at University of Cambridge) along with an analytical method in order to cross-check the validity of the results. The results are compared through various airgaps and frequencies showing excellent quantitative and qualitative agreement. We observe that the current charging curve contains ripples within each cycle, which cannot be captured via the analytical method. Such ripples cause ripple AC loss in the HTS dynamo, which is shown to be almost constant during the whole charging process. These ripples could also produce significant ripple current amplitude and AC loss associated to them.

We also present the first 3D model of an HTS flux pump. Employing MEMEP 3D,

the performance of an HTS dynamo is investigated and analyzed in open-circuit mode. We study the screening current distribution across the tape surface in several key positions of the magnet movement for generating voltage. It is found that, while the magnet traverses on top of the tape, the maximum value of the component of the electric field along the tape length E_y , is much larger than the component along the tape width E_x , which highlights the role of J_y to generate the voltage throughout the tape surface. In addition, the average E_x in the whole sample vanishes because of symmetry. We also study the effect of the tape length on voltage generation in the flux pump and discover that the distance between voltage taps for precise measuring of the voltage depends on not only the diameter of the magnet but also the distance between magnet and tape surface. Finally, the calculated modeling results are compared against experiments for several airgaps, which show very good agreement. Indeed, the agreement with measurements is better for 3D modeling than 2D, since 3D modeling can take the real shape of the cylindrical magnet into account.

2. Calculation methods

2.1. MEMEP 3D method

In this work, we use MEMEP 3D to model the HTS dynamo in three dimensions. In MEMEP method, the solution minimizes the entropy production made by electromagnetic fields [2,3]. The MEMEP 3D is a variational method based on \mathbf{T} -formulation and is able to exploit several strategies to speed up calculation such as parallel computing, dividing into sectors and symmetry. Since the current density \mathbf{J} and \mathbf{T} only exist inside the material, in contrast to conventional finite-element methods, meshing is only needed in this region, increasing the calculation speed significantly [3].

MEMEP is based on the calculation of current density, \mathbf{J} , by minimizing a functional containing magnetic vector potential \mathbf{A} , and current density \mathbf{J} . It has been proved that the minimum of this functional in the quasimagnetostatic limit is the unique solution of the Maxwell differential equations [3]. This method is able to take materials with nonlinear $\mathbf{E}(\mathbf{J})$ relation such as superconductors into account, including the multi-valued $\mathbf{E}(\mathbf{J})$ relation of the critical-state model.

The relation between the current density and the vector and scalar potentials is as follows:

$$\mathbf{E}(\mathbf{J}) = -\frac{\partial \mathbf{A}}{\partial t} - \nabla \varphi, \quad (1)$$

and the current conservation equation:

$$\nabla \cdot \mathbf{J} = 0, \quad (2)$$

where $\partial \mathbf{A} / \partial t$ is the change of vector potential with respect to time and φ is the scalar potential. For Coulomb's gauge ($\nabla \cdot \mathbf{A} = 0$), the vector potential \mathbf{A} in Equation (1) includes the contributions from the applied field \mathbf{A}_M and the current density in the superconductor \mathbf{A}_J .

For magnetization problems, the method uses the effective magnetization \mathbf{T} as state variable, defined as

$$\nabla \times \mathbf{T} = \mathbf{J} \quad (3)$$

and $\mathbf{T} = 0$ outside the sample. Configurations with transport current are possible after adding an additional term to the equation above [3].

Equation (2) is always satisfied because $\nabla \cdot (\nabla \times \mathbf{T}) = 0$. Thus, we only need to solve equation (1). In addition, the Coulomb's gauge has been assumed and hence the scalar potential φ becomes the electrostatic potential [4].

Based on Faraday's law, the relation between electric field \mathbf{E} and magnetic field density \mathbf{B} is as follows

$$\nabla \times \mathbf{E} = -\partial \mathbf{B} / \partial t. \quad (4)$$

The vector potential \mathbf{A} in the functional has two contributions including \mathbf{A}_M and \mathbf{A}_J standing for the vector potential due to the applied field and the vector potential due

to the current density in the superconductor, respectively. The \mathbf{A}_M component can be replaced by the vector potential due to the magnet in a dynamo, while \mathbf{A}_J is calculated with the following volume integral of current density

Solving Faraday's law (Equation (4)) is equivalent to minimizing the following functional

$$F = \int_{\Omega} d^3\mathbf{r} \left[\frac{1}{2} \frac{\Delta \mathbf{A}_J}{\Delta t} \cdot \Delta \mathbf{J} + \frac{\Delta \mathbf{A}_M}{\Delta t} \cdot \Delta \mathbf{J} + U(\mathbf{J}_0 + \Delta \mathbf{J}) + \nabla \varphi \cdot (\mathbf{J}_0 + \Delta \mathbf{J}) \right], \quad (5)$$

where Ω is the superconducting or normal conducting region in the 3D space, $\Delta \mathbf{J}$, $\Delta \mathbf{A}_J$, $\Delta \mathbf{A}_M$ are the change of the variable between two consecutive time steps, Δt is the time difference between two time steps, and \mathbf{J}_0 is the current density at the previous time step. However, in the case of open-circuit with zero transport current, the functional becomes:

$$F = \int_{\Omega} d^3\mathbf{r} \left[\frac{1}{2} \frac{\Delta \mathbf{A}_J}{\Delta t} \cdot \Delta \mathbf{J} + \frac{\Delta \mathbf{A}_M}{\Delta t} \cdot \Delta \mathbf{J} + U(\mathbf{J}_0 + \Delta \mathbf{J}) \right]. \quad (6)$$

In addition, U in this functional is the dissipation factor, defined as [3]

$$U(\mathbf{J}) = \int_0^{\mathbf{J}} \mathbf{E}(\mathbf{J}') \cdot d\mathbf{J}'. \quad (7)$$

This dissipation factor can include any E - J relation in superconductors or normal conductors.

We can rewrite the 3D functional as a function of \mathbf{T} based on Equation (3) as

$$L = \int_V dv \left[\frac{1}{2} \frac{\Delta \mathbf{A}_J}{\Delta t} \cdot (\nabla \times \Delta \mathbf{T}) + \frac{\Delta \mathbf{A}_M}{\Delta t} \cdot (\nabla \times \Delta \mathbf{T}) + U(\nabla \times \mathbf{T}) \right] \quad (8)$$

To solve the problem in time dependent mode, the functional is minimized in discrete time steps. One of the key points of the \mathbf{T} -formulation is that it is not necessary to take the scalar potential φ into account, greatly simplifying the problem in 3D.

2.1.1. Mesh definition The optimum number of mesh for a tape with dimensions $12 \times 48 \times 0.001$ mm is chosen as $50 \times 60 \times 1$ along the x , y and z axis, respectively, inside the superconductor. The calculation time for this configuration taking the $J_c(B, \theta)$ dependency into account and meshes $50 \times 200 \times 1$ and $50 \times 60 \times 1$ is around 16 hours and 40 minutes and less than 3 hours, respectively, on a desktop workstation with two Intel(R) Xeon(R) CPUs of E5-2630 v4 @2.20GHz with 20 virtual cores (10 physical cores) each and 64 GB RAM. For the case of constant J_c with $50 \times 200 \times 1$ mesh the computation reduces to around 6 hours and 40 minutes.

2.2. MEMEP 2D method

In this work, we also employed the MEMEP 2D method in two dimensions for modeling the flux pump in open-circuit mode and in the case of charging a coil. We extend the numerical method in [2, 3] in order to take lumped circuit elements such as inductances and resistances into account.

The functional in Equation (6) still can be used in the case of connection of the superconducting tape in series with a coil. In this case, Ω includes the superconducting tape, the coil and any series connected resistance (joints, coil resistance and so on). With the assumption of the coil, resistance and the tape being far away from each other, the magnetic field and vector potential of each component does not affect the other. Therefore

$$F = F_S + F_L + F_R, \quad (9)$$

where F_S , F_L , F_R are the terms (of a single functional) for the superconducting tape, coil, and resistance, respectively. These terms are the same as in Equation (6) if we replace Ω by Ω_S , Ω_L and Ω_R , being the 3D regions for each part. Next, with the following assumptions, we are able to simplify the 3D formulation of these functionals.

Taking these relations into account and Equation (1), we find that:

$$\nabla\varphi(\mathbf{r}) = \frac{\partial\varphi}{\partial z} \mathbf{e}_z, \quad (10)$$

where $\partial\varphi/\partial z$ is uniform within the superconductor.

The voltage V is conventionally defined as in a passive circuit element $V = \varphi(z = -l/2) - \varphi(z = +l/2)$. With these assumptions, the superconducting tape functional can be simplified as

$$F_S = l \int_{S_S} d^2\mathbf{r}_2 \left[\frac{1}{2} \Delta J \frac{\Delta A_J}{\Delta t} + \Delta J \frac{\Delta A_M}{\Delta t} + U(J) \right] - V_S I, \quad (11)$$

where S_S is the cross-section of the superconducting tape, I is the net current in the tape, A_M is the vector potential caused by the external magnetic field due to the rotating magnet in the flux pump, which has the non-uniform applied magnetic field \mathbf{B}_M .

In here and for simplicity, we assume an ideal inductor with inductance L , although in our method, it is also possible to consider a superconducting coil with local non-linear resistivity. Thus, we neglect (non-linear) eddy currents and any linear or non-linear resistive effect in the wire. Therefore, \mathbf{J} is uniform in the wire cross-section and $U(\mathbf{J}) = 0$. Considering this fact that the coil is not exposed to any external magnetic field, the coil functional from the Equation (6) reduces to

$$F_L = \frac{1}{2} L \frac{(\Delta I)^2}{\Delta t} - V_L I, \quad (12)$$

where the voltage of the inductance V_L , is conventionally defined as in a passive circuit element, which is defined as the difference in electrostatic potential between the entry and exit of current I at the coil terminal.

Similarly for the resistance, we assume no eddy currents in the linear resistance, and that they are not submitted to external applied magnetic fields. Following the reasoning of [5], we find that the resistance functional from the Equation (6) reduces to

$$F_R = \frac{1}{2}RI^2 - V_R I \quad (13)$$

for any 3D shape of the resistive joint, where R is the resistance and the voltage V_R is defined as in a passive circuit element.

Since all elements are connected in series in a closed circuit, they follow Kirchhoff's second law $V_S + V_L + V_R = 0$. Thus, the whole system minimizes the following functional

$$F = l \int_{S_S} d^2 \mathbf{r}_2 \left[\frac{1}{2} \Delta J \frac{\Delta A_J}{\Delta t} + \Delta J \frac{\Delta A_M}{\Delta t} + U(J) \right] + \frac{1}{2} L \frac{(\Delta I)^2}{\Delta t} + \frac{1}{2} RI^2. \quad (14)$$

Here, we have used the same voltage definition for all elements, as a passive circuit element, for consistency. However, if we consider the HTS dynamo as a voltage source, the voltage is defined with opposite sign.

2.2.1. Mesh definition For modeling in 2D, meshing was performed only inside the superconductor region in rectangular shape elements and uniformly across the object.

For open-circuit mode, only one element along the thickness of the superconducting tape suffices. Therefore, the whole number of elements in the modeling was between 200 to 800 elements, which reduces the computation time significantly compared to conventional FEM.

For the case of charging a coil, we have used 60 mesh elements across the width and one mesh element along the thickness of the tape. We have limited the number of mesh elements as much as possible up to a point that does not affect the accuracy of the results. The reason was to reduce the calculation time in order to be able to calculate up to millions of time steps in a reasonable time.

2.3. HTS tape resistivity

To describe the non-linear superconductor characteristic, the model uses the isotropic $E - J$ power law

$$\mathbf{E}(\mathbf{J}) = E_c \left(\frac{|\mathbf{J}|}{J_c} \right)^n \frac{\mathbf{J}}{|\mathbf{J}|}, \quad (15)$$

where $E_c = 10^{-4}$ V/m is the critical electric field, J_c is the critical current density and n is the power law exponent or n-value, which defines the steepness of the transition between the superconducting state and the normal state.

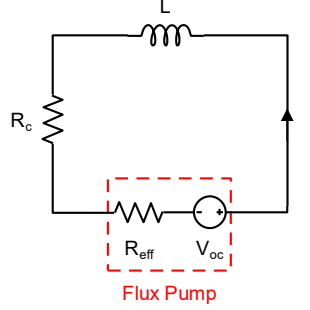


Figure 1: Equivalent electrical circuit model of an HTS dynamo connected to a coil via soldered joints.

2.4. Analytical method for coil charging

For many configurations [6, 7], the DC current-voltage relation of the flux pump is linear (see, for example, modeled results from MEMEP in Figure 6), and hence it can be modeled as a DC voltage source in series with an internal effective resistance, R_{eff} , as shown in Figure 1. The value of the voltage source is equal to DC open-circuit voltage of the dynamo V_{oc} , which is the DC value of the output voltage when the transport current is zero. During the operation, a coil with inductance L is connected via the circuit resistance R_c (resistance of soldered joints) to the dynamo. Therefore, the coil can be treated as an independent LR circuit, which is charged via the voltage source.

The current in the electrical circuit of Figure 1 can be obtained using the following equation obtained by solving the governing equation of the circuit [8]

$$i(t) = I_{sat} [1 - e^{t/\tau}], \quad (16)$$

where $I_{sat} = V_{oc}/(R_c + R_{\text{eff}})$ is the saturation current, which is the maximum value of current that the flux pump can deliver and $\tau = L/(R_c + R_{\text{eff}})$ is the time constant in the circuit, determining the charging rate of the flux pump. The flux pump reaches 99.3% saturation of the final value, I_{sat} , after 5τ .

3. General Definitions

Considering $V = -l \cdot \partial_z \phi$ and $-\partial_z \phi = E(x, y) + \partial_t A(x, y)$ for any (x, y) , we define the cumulative total output voltage $V_{cumul}(t)$, as:

$$V_{cumul}(t) = \int_0^t V(t') dt'. \quad (17)$$

where $V_{cumul}(t)$ is the magnetic flux in the coil connected to the flux pump, due to Faraday's law. Since the magnetic flux is $\phi = L \cdot I$, this magnetic flux, or cumulative voltage, is proportional to the inductance L of the coil connected to the flux pump.

The DC output voltage of the dynamo V_{DC} , is:

$$V_{DC} = \frac{1}{T} \int_t^{t+T} V(t') dt', \quad (18)$$

as the time average value of the induced voltage over one period of rotation, T , in the steady-state.

The cumulative DC output voltage $V_{DC,cumul}(t)$, is:

$$V_{DC,cumul}(t) = \int_0^t V_{dc}(t') dt'. \quad (19)$$

The DC output voltage can be rewritten as:

$$V_{DC} = fl \int_0^{1/f} [\partial_t A + E(J)] dt = fl \int_0^{1/f} E(J) dt = fl \int_0^{1/f} \rho(J) J dt \quad (20)$$

where l is the tape length and ρ is the non-linear resistivity of HTS tape. In the equation above, the vector potential in steady state is used, which is periodic and hence $\int_0^{1/f} \partial_t A dt = A(x, y, t = 1/f) - A(x, y, t = 0)$. The cause of the periodicity of vector potential is that both A from the magnet and the currents in the superconducting tape are periodic after the first cycle.

Based on Equation (20), the output V_{DC} only depends on the electric field generated by the resistivity of the HTS tape, which itself is a function of the tape current density. An interesting feature is that V_{DC} can be calculated from the time integral of $\rho(J)J$ on any point and the integrals for all points yielding the same result. Then, we can also use the cross-section average of the electric field $\mathbf{E}(\mathbf{J})$ to calculate V_{DC} , being

$$E_{av}(t) = \frac{1}{S} \int_{S_S} d^2 \mathbf{r}_2 \rho[J(\mathbf{r}_2)] J(\mathbf{r}_2), \quad (21)$$

where S is the cross-section surface, dS is its differential and ρ is the nonlinear resistivity of the HTS tape.

Using the same arguments as Equation (20), we find that the DC voltage follows

$$V_{DC} = fl \int_0^{1/f} E_{av}(J) dt. \quad (22)$$

For a linear material we have

$$E_{av}(J) = \rho J_{av} = \rho \frac{I}{S}, \quad (23)$$

and hence V_{DC} vanishes for the open-circuit case because $I = 0$. However, V_{DC} does not vanish for the superconductor non-linear $E(J)$ relation.

For the infinitely long configuration of figures 2 and 5, the total output voltage of the flux pump $V(t)$ is comprised of three components:

$$V(t) = -l \cdot \partial_z \varphi = l \cdot [E_{av}(J) + \partial_t A_{av}] = l \cdot [E_{av}(J) + \partial_t A_{M,av} + \partial_t A_{J,av}], \quad (24)$$

where l is the tape length, φ is the electrostatic potential, E_{av} is obtained by Equation (21), $A_{M,av}$ and $A_{J,av}$ are the average magnetic vector potential over the tape cross-section due to the permanent magnet and the screening current in the superconducting tape, respectively. Since for the infinitely long geometry $\partial_z\varphi$ is uniform within the superconductor, this quantity can be expressed as a function of the average over the tape cross-section of $E(J)$ and $\partial_t A$, $E_{av}(J)$ and $\partial_t A_{av}$, respectively.

Among these three terms, only E_{av} is not periodic within a cycle leading to a DC voltage value and thus the pumping phenomenon. The two other terms $A_{M,av}$ and $A_{J,av}$ are periodic within a cycle and do not have any effect on the DC voltage value [9,10]. However, they cause a significant ripple in the voltage, and consequently also a ripple in the current signal in the coil connected in series, resulting in AC loss in the superconducting coil and other dynamic effects.

The output voltage difference between the tape at 77 K (superconducting mode) and at 300 K (normal mode) is

$$\Delta V = V_{77\text{K}} - V_{300\text{K}}, \quad (25)$$

which is equal to

$$\Delta V = l \left[\partial_t (A_{av,J,77\text{K}} - A_{av,J,300\text{K}}) + E_{av}(J) - \rho_{300\text{K}} \frac{I}{S} \right]. \quad (26)$$

For open-circuit mode, the last term vanishes. In addition, since the metal resistivities are large at 300 K, the vector potential generated by currents at 300 K ($A_{av,J,300\text{K}}$) will be negligible compared to those from superconductor at 77 K ($A_{av,J,77\text{K}}$). Therefore we will have

$$\Delta V_{oc} \approx l [\partial_t A_{av,J} + E_{av}(J)], \quad (27)$$

where the sub-index *oc* denotes the open-circuit mode.

4. Open-circuit case results

In this section, we present the results of the 2D modeling in open-circuit case including the investigation of the main behavior of HTS dynamo, effect of tape critical current, airgap and magnet geometry on DC voltage generation and comparison to experiments. Figure 2 (a) shows the sketch of the problem configuration used for the case of open-circuit HTS dynamo.

4.1. Main behavior of HTS dynamo

The results presented in this section were calculated for airgap of 3.3 mm. The voltage was calculated considering the $J_c(B, \theta)$ dependence. Besides, all the results belong to the second cycle to skip the transient state in the first cycle.

Figure 2 (b) shows the total output voltage, $V(t)$ for the modeled flux pump, Figure 2 (c) shows the generated voltage by the non-linear resistivity of the HTS tape, E_{av} . By calculating the voltage DC value of graphs in Figures 2 (a) and 2 (b), it is observed that the flux pump generates a voltage DC value equal to $37.24 \mu\text{V}$, which is responsible for energizing the superconducting coil connected to the pump. Over many cycles, this value of DC voltage will be accumulated to inject the magnetic flux into a superconducting circuit connected in series with the pump called $V_{DC,cumul}$ [1]. Figure 2 (d) shows this trend over 10 cycles for the modeled flux pump.

4.2. Effect of tape critical current

In here, we investigate the impact of the critical current density of the HTS tape on the generated open-circuit voltage of the flux pump. We consider several different cases with constant J_c with critical currents ranging from 70 to 1120 A, including the experimental critical current in self-field of 280 A. The rest of the parameters are the same as in the previous sections. Figure 3 (a) shows the signal of $E_{av} \cdot l$ for three different values of J_c corresponding to critical currents of 140, 280 and 560 A. An important result is that this signal is almost the same, taking into account the high variation of J_c . The cause is that, as long as the tape is saturated with magnetization currents, only the value and time dependence of the magnetic field from the magnet is important. When looking at the DC component, which is responsible for flux pumping, the difference is even smaller being almost no difference for I_c between 70 to 560 A.

4.3. Airgap dependence of open-circuit voltage

The input parameters used for these calculations were obtained from [1], so that it can be comparable to the experimental results presented in the mentioned paper.

We may wonder what is the boundary for generating voltage in a flux pump. In other words, what is the maximum airgap that results in non-zero voltage in the flux pump. This issue is directly related to the value of magnetic flux density on the tape surface. Figure 3 (b) demonstrates the change of open-circuit DC voltage generated in the modeled flux pump for airgaps up to 50 mm. That figure indicates that even in airgaps as large as 50 mm, DC voltage still exists; while the maximum applied perpendicular magnetic field density is of only 7 mT. Although this value is insignificant, i.e. around $0.0002 \mu\text{V}$, it suggests that there is still voltage generated in the flux pump. Considering the fact that the maximum perpendicular magnetic field density of 7 mT is much less than the penetration field (B_p) estimated for the modeled HTS tape in the flux pump (i.e. 25 mT) [11], it can be concluded that the generation of voltage in flux pump does not require full penetration of the field into the tape, but only partial penetration can lead to voltage generation.

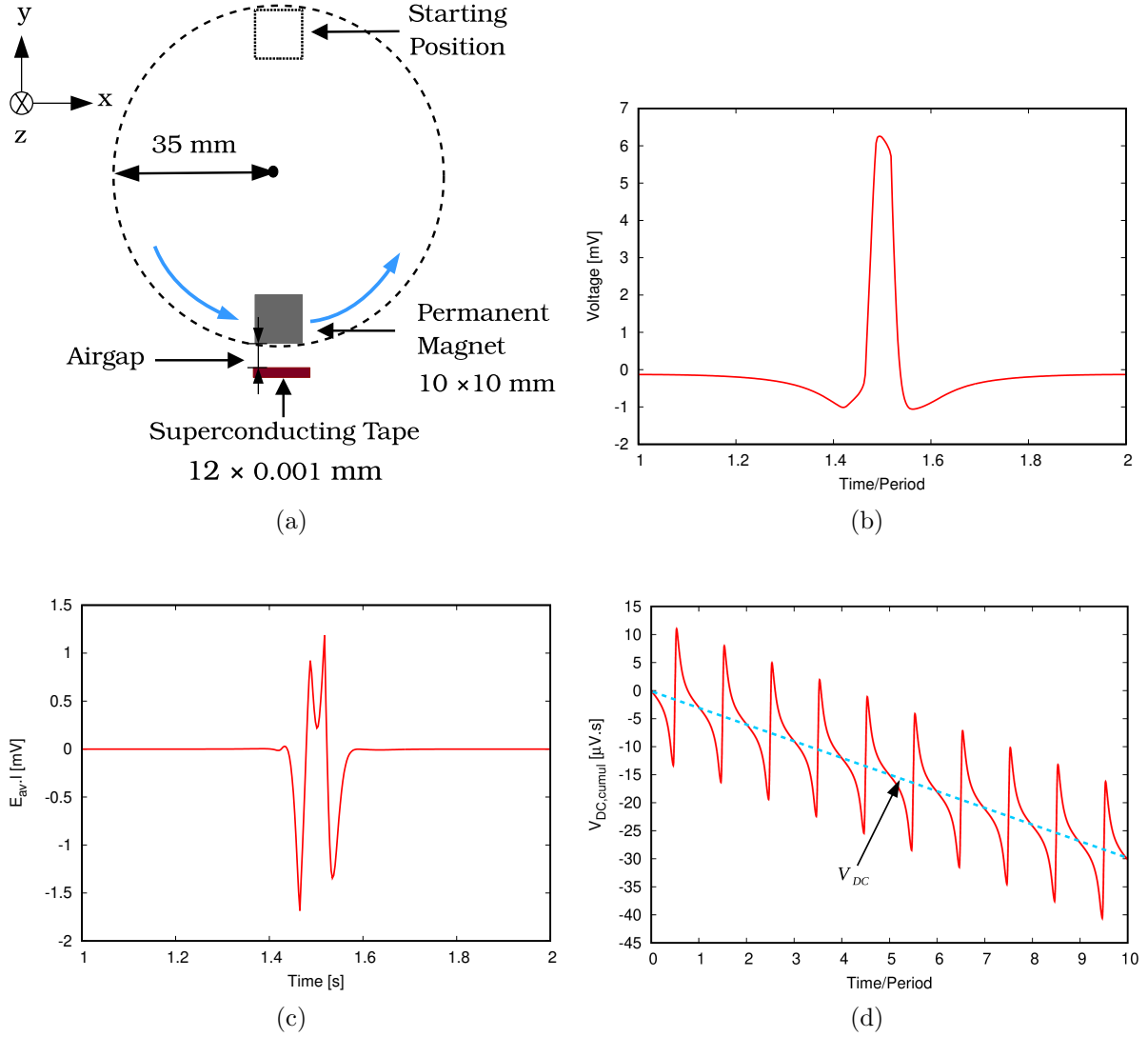


Figure 2: (a) The 2D model configuration above is sufficient to describe the main features of a dynamo-type flux pump in open-circuit case. The magnet and superconductor are assumed infinite in the z direction. (b) Total calculated output open-circuit voltage $V(t)$ for the modeled flux pump in 2D and for the airgap of 3.3 mm, with assumption of $J_c(B, \theta)$ dependence. (c) The calculated open-circuit voltage E_{av} , generated by the non-linear resistivity of the HTS tape, for the modeled flux pump in 2D and for the airgap of 3.3 mm, with assumption of $J_c(B, \theta)$ dependence. (d) Accumulated open-circuit voltage, $V_{DC,cumul}$ over 10 cycles for the modeled flux pump in 2D and for the airgap of 3.3 mm, with assumption of $J_c(B, \theta)$ dependence.

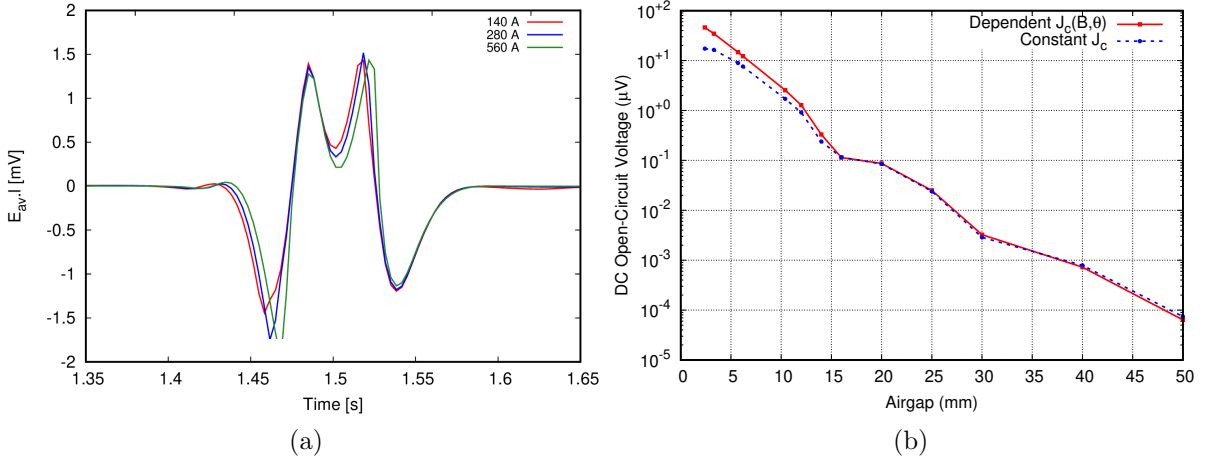


Figure 3: (a) Comparison of the generated open-circuit voltage, $E_{av} \cdot l$, in the airgap of 3.3 mm for tapes with different J_c , corresponding to the I_c values in the legend. The signal is for the second cycle, in order to skip the transient. (b) Although the DC open-circuit voltage in the flux pump decreases with the airgap, it never vanishes. Calculated voltage for the cases of constant J_c and magnetic-field dependent $J_c(B, \theta)$ for airgaps in the range of 2.4 to 50 mm.

4.4. Impact of Magnet Geometry on Open-Circuit Voltage

We also study the impact of changing magnet size (with equal width and height) on the open-circuit voltage of the modeled flux pump. The configuration of the modeled flux pump are the same as described in section 4. The variable parameters are the dimensions of the magnet including magnet width (along x axis) and magnet height (along y axis) (see Figure 2). Figure 4 (red curve with round symbols) shows the calculated open-circuit DC voltage of the modeled flux pump with increasing the magnet size from 3 mm to 20 mm. As it is clear, the open-circuit voltage increase continuously with increasing the dimension of the magnet. The qualitative behaviour of dynamo-type flux pump with HTS superconductor is very different than LTS type I superconducting flux pumps, where the size of the magnet should be smaller than the tape. Here, magnets largely exceeding the size of the magnet should be smaller than the tape. Here, magnets largely exceeding the tape width provide relatively large flux pumping as it is shown in Figure 4.

One reason for the continuous increasing of the open-circuit voltage is the continuous increasing of the maximum magnetic field density on the tape surface. Figure 4 (the blue curve with square symbols) shows the trend of increasing the y component of maximum magnetic field density, $B_{y,max}$, perpendicular to the tape surface. This value raises continuously (but not linearly) as the magnet become larger in size, so as the open-circuit voltage. The other reason is connected to the role of overcritical currents in creating voltage.

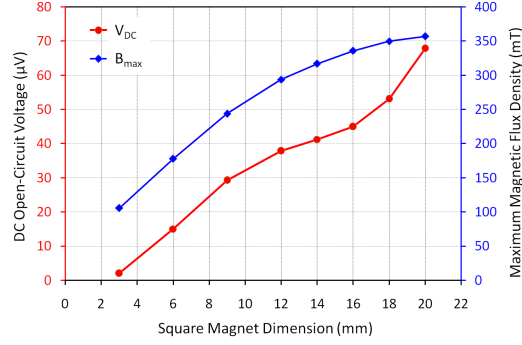


Figure 4: The open-circuit DC voltage of the modeled flux pump with increasing the magnet size (with equal width and height) from 3 mm to 20 mm for 3.7 mm airgap and assumption of $J_c(B, \theta)$ dependence.

5. Coil charging case results

The results of calculations for charging a coil by an HTS dynamo using the MEMEP method, calculated at Institute of Electrical Engineering, Slovak Academy of Sciences, and segregated \mathbf{H} -formulation finite-element method (SEG-H) [12, 13], implemented in COMSOL Multiphysics and calculated at Department of Engineering, University of Cambridge along with analytical results are presented and discussed in this section. We use two different methods along with an analytical method for our calculations in order to cross-check the validity of the results. Fig. 5 shows the configuration of the studied problem.

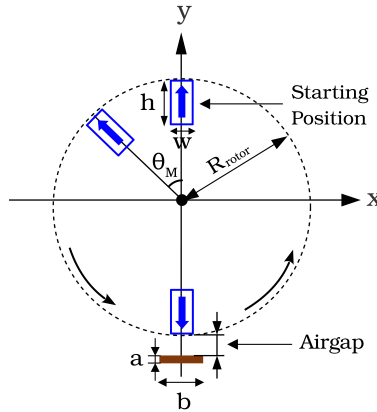


Figure 5: Configuration of the studied problem in the xy -plane, based on the benchmark HTS dynamo problem [13].

5.1. I - V Curve

Using the I - V curve, the HTS flux pump can be described as a current-controlled voltage source. This means that for different transport DC currents, the flux pump outputs different DC voltage values based on its effective resistance.

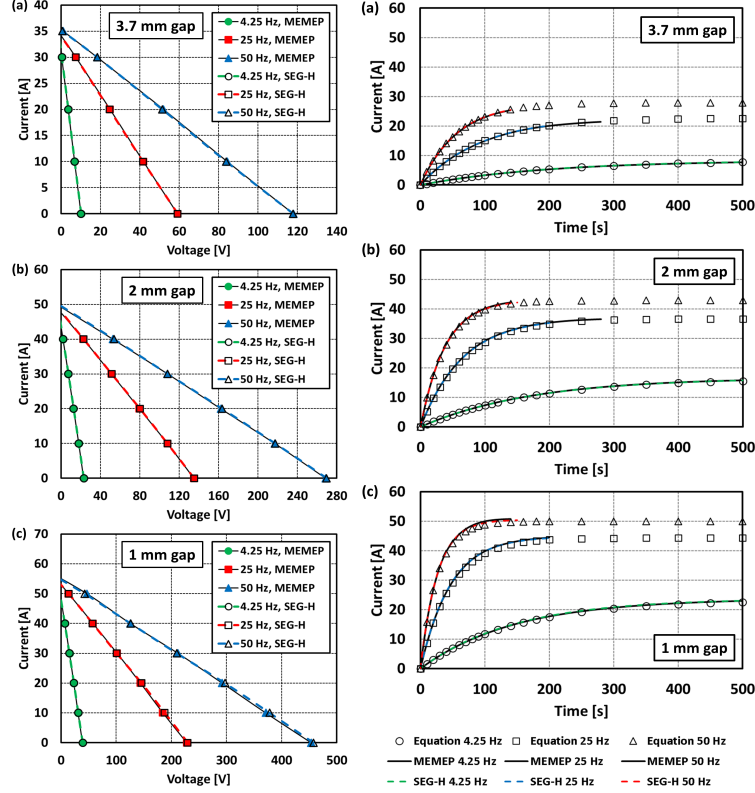


Figure 6: (left) I - V curves of the modeled HTS dynamo calculated by MEMEP and SEG-H methods for three frequencies of 4.25, 25 and 50 Hz and for airgaps of (a) 3.7 mm, (b) 2 mm, (c) 1 mm. (right) The calculated charging current curves of the coil for three frequencies of 4.25, 25 and 50 Hz for airgaps of (a) 3.7 mm, (b) 2 mm, (c) 1 mm.

Figure 6 (left) shows the I - V curves of the modeled HTS dynamo calculated by the two numerical methods for three frequencies of 4.25, 25 and 50 Hz and three airgaps of 1, 2 and 3.7 mm. The results verify the fact already shown by experiments that R_{eff} , being the slope of the I - V curve of the flux pump, for a fixed rotation frequency and superconducting operating regime has a constant value and is not a function of the current, which depends on the characteristic of the flux pump. In addition, the open-circuit voltage V_{oc} and the slope of the I - V curves, which describe the effective resistances of the dynamo, increase directly proportional to the frequency. Regardless of the airgap value, the two compared methods have excellent agreement at low frequencies and with increasing the frequency, this agreement deteriorates slightly.

5.2. Instantaneous current

Figure 7(a) shows the dynamic charging of the coil for the first five cycles of the case with a 3.7 mm airgap and a frequency of 25 Hz for the two studied models, which again have excellent agreement. The charging current curve contains ripples that resembles the ripples of cumulative total output voltage $V_{cumul}(t)$ of the HTS dynamo.

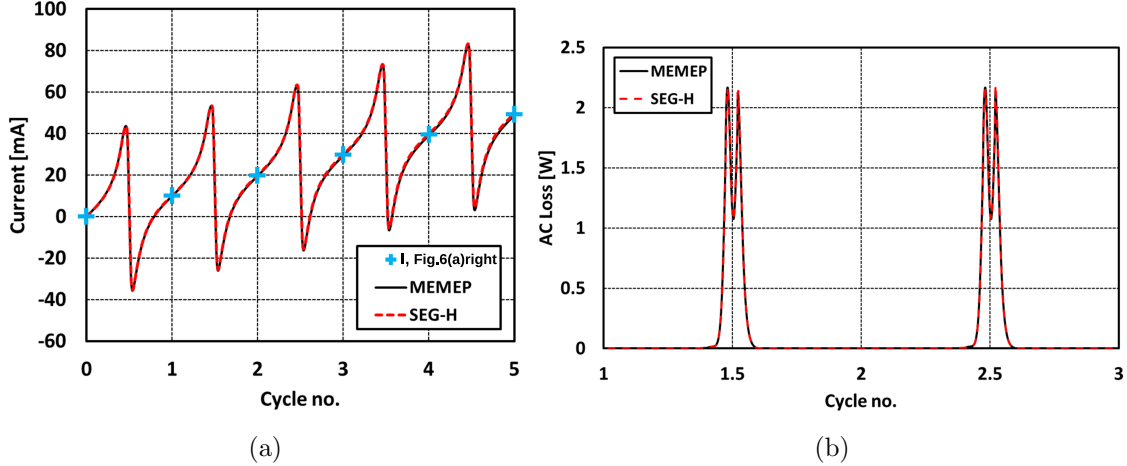


Figure 7: (a) Dynamic charging current curve of the modeled coil over the first five cycles for the two studied models. The cross symbol refers to the extracted data points at the end of each cycle used for plotting Figure 6. The case belongs to 3.7 mm airgap and 25 Hz frequency. (b) Ripple AC loss in the modeled coil over the second and third cycles for the two studied models. The case belongs to the 3.7 mm airgap and 25 Hz frequency.

The ripples of the charging curve shown in Figure 7(a) generate AC loss in the coil, which is shown in Figure 7(b). We calculated the average AC loss in the first five charging cycles (ignoring the first transient cycle) for the MEMEP method as 135.4 mW and for SEG-H method as 135.7 mW. The average AC loss of the 5001st, close to saturation of pumping, for the MEMEP method is 135.7 mW and for SEG-H method is 135.9 mW. This suggests that the ripple AC loss for a given frequency is almost constant during the whole charging period of the coil.

5.3. Charging Behavior

Figure 6 (right) shows the calculated transport currents as a function of time for airgaps of (a) 3.7 mm, (b) 2 mm and (c) 1 mm with rotation frequencies of 4.25, 25 and 50 Hz, comparing the results of the two numerical methods with the analytical ones. Figure 6 (right) shows that for a given frequency, the coil current saturates at a higher value and in less time as the airgap decreases. For a given airgap, the coil current saturates faster with a higher value of I_{sat} as the frequency increases.

6. 3D modeling case results

Fig. 8 shows the configuration of the 3D model in 2 different views. The magnet rotates in the xz -plane on top of the tape in counter clockwise direction. The magnet magnetization is pointed out to the outside of rotation circle.

6.1. Current and Electric Field Analysis

In this section, all the modeling results have been calculated and presented using constant J_c , since it eliminates the complications of J_c variations due to inhomogeneous magnetic field from the magnet and simplifies the performance study of the dynamo. Later, in section 6.3, we take the $J_c(B, \theta)$ dependence into account.

To examine better the flux pump behavior, we defined several key positions of the magnet while traversing the HTS tape. Figure 9 (b) displays the current density (maps of the modulus and current lines) for key magnet positions (see Figure 9 (a)). Step 0 belongs to the beginning of second cycle when the magnet is still far away from the tape and the tape is fully saturated with screening currents remained from the first cycle. At step A, the magnet projection touches the tape and starts to enter it from the left side. At step B, half of the magnet has entered the tape and the magnet magnetic field has occupied the whole tape. Thus, the overcritical currents can be observed throughout the tape. At step C, the magnet has reached the middle of the tape while the tape is still fully occupied with overcritical screening currents. The screening currents direction has been altered compared to step B due to the tendency of the change in the magnetic field from increasing mode to decreasing mode. At step D, the situation is similar to step B but with opposite direction of overcritical screening currents. At step E, while the magnet is leaving the tape, the tape is still fully saturated with overcritical screening currents and the direction of these currents are the same as step 0.

Figure 10 (b) depicts electric field maps related to the key magnet positions of Figure

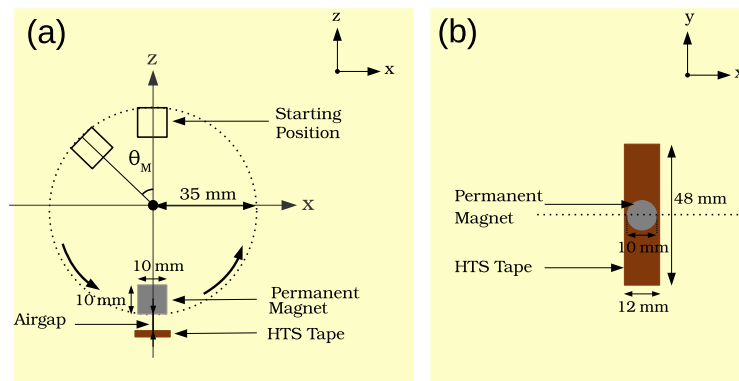


Figure 8: Configuration of the 3D model: (a) view from xz -plane, (b) view from xy -plane.

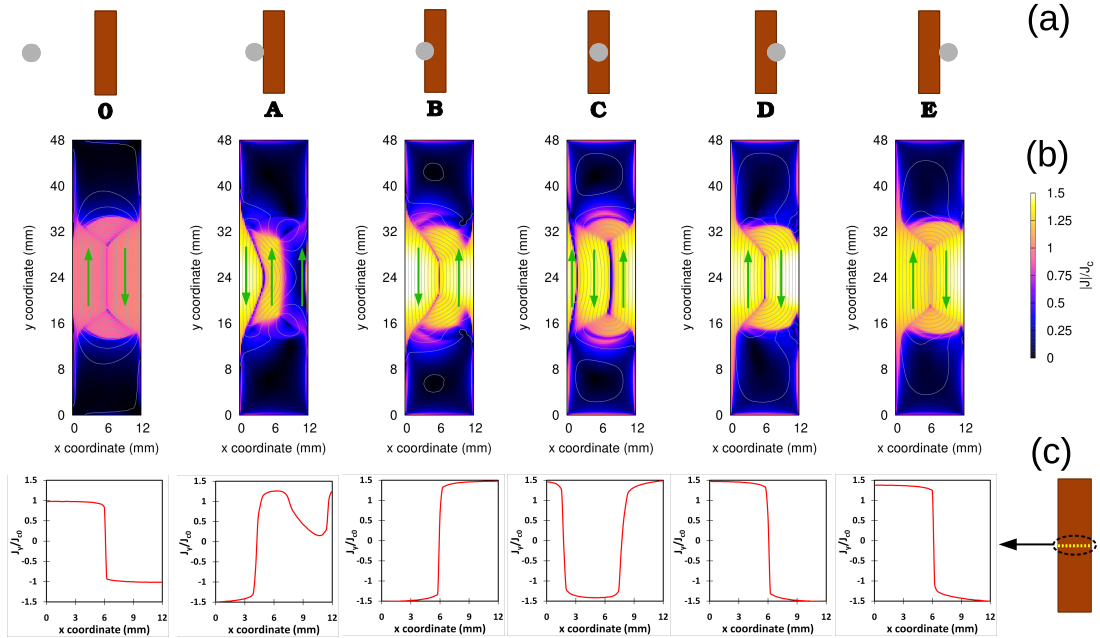


Figure 9: Current modeling results for airgap 3.3 mm and constant J_c . (a) Key magnet positions, (b) Current modulus maps and current lines, (c) Current profiles of J_c -normalized J_y in the mid-plane of the tape ($y = 24$ mm). At the mid-plane, J_x vanishes by symmetry.

10 (a) and Figure 10 (c) shows the profiles of the y component of the electric field, E_y , in the middle of the tape length (the E_x component vanishes there). The main area in the tape responsible to generate voltage in the tape lies under and along the magnet cross section (area from 19 mm to 29 mm along y axis), where the magnet is traversing. At steps B and D the largest yellow areas are observed, showing the high values of electric field induced in these areas (around 0.4 V/m).

In Figure 11, we study the x and y components of the current density and electric field in more detail in a certain time step (step C). In Figure 11 (a) it is obvious that J_x stays just below the critical current while J_y reaches up to 1.5 times of J_c [see Figure 11 (b)]. As a result, E_y is almost 20 times higher than E_x [see Figure 11 (c) and Figure 11 (d)]. In addition, since J_x is symmetric along the length, E_x is also symmetric [see Figures 11 (a) and (c)]. Thanks to this symmetry, the average E_x in the whole sample vanishes, and thence E_x does not contribute to the voltage.

6.2. Impact of Tape Length on Voltage Generation

Studying the impact of the tape length on voltage generation assists us to realize what is the minimum efficient tape length (along the y axis) that can be employed in a flux pump. From another point of view, this study help us to select the proper distance between

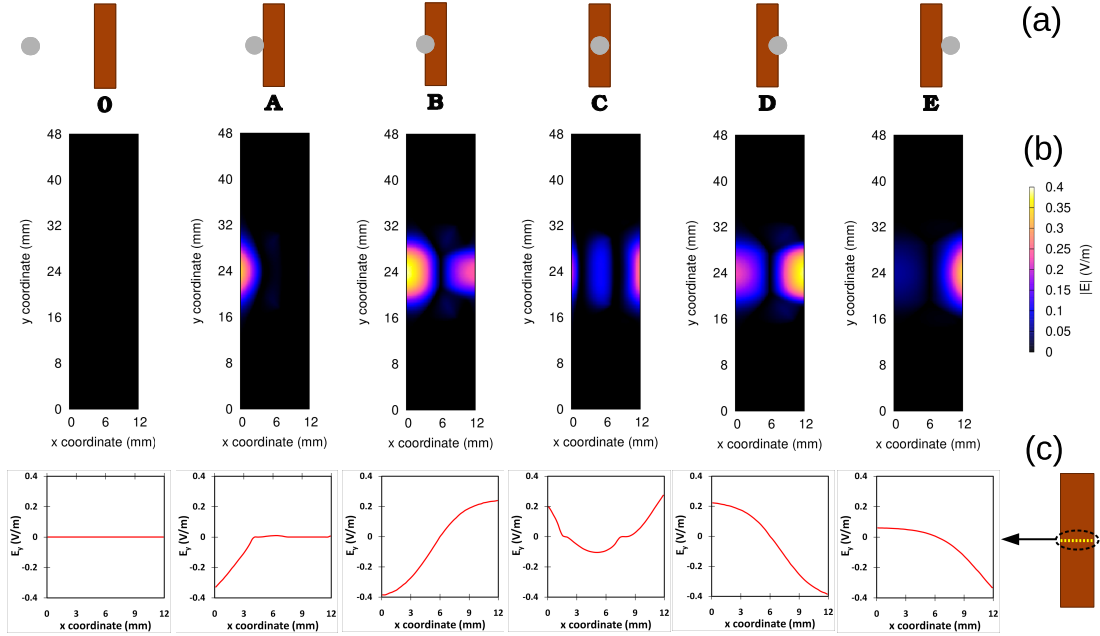


Figure 10: Electric Field modeling results for airgap 3.3 mm and constant J_c . (a) Key magnet positions, (b) Electric field modulus maps, (c) Electric field profiles of E_y regarding the key magnet positions in the mid-plane of the tape ($y = 24$ mm). E_x at the mid-plane vanishes due to symmetry.

voltage taps while measuring the voltage signals in a flux pump. This distance is of course a variable of magnet dimension, especially along the length. In this section, we studied this effect with the same flux pump configurations for various airgaps. Now, we use $J_c(B, \theta)$ dependence in order to obtain a realistic description that is closer to experiments. The tape length, changing between 5 mm to 48 mm, and the airgap, varying from 1 mm to 10 mm, are chosen as variables while the frequency is kept constant as 12.3 Hz.

Figure 12 (a) shows the result of ΔV normalized by the frequency against the magnet angle θ_M for different tape lengths and for 3.3 mm airgap. It is clear that above 20 mm length, the results of ΔV remain almost the same and the curves coincide to each other. Also, Figure 12 (b) shows the DC open-circuit voltage value versus tape length for various airgaps, from 1 mm to 10 mm. Up to the airgap of 6 mm, the DC voltage changes only a few percent with increasing the tape length from 24 to 48 mm. This can be justified by the distribution of current modulus on the tape surface for different airgaps, shown in Figure 12 (c). In this figure, the dashed green rectangles show the area on the tape surface containing the flow of y component of current density, J_y , that is responsible for creation of voltage in the tape. Almost all of the created voltage in the tape is generated in this area. This fact also can be recognized in Figure 12 (b) by the decrease in the slope of the curves from 1 mm to 10 mm airgap, showing that in smaller airgaps, the induced voltage is more concentrated in the center of the tape, where the magnet traverses.

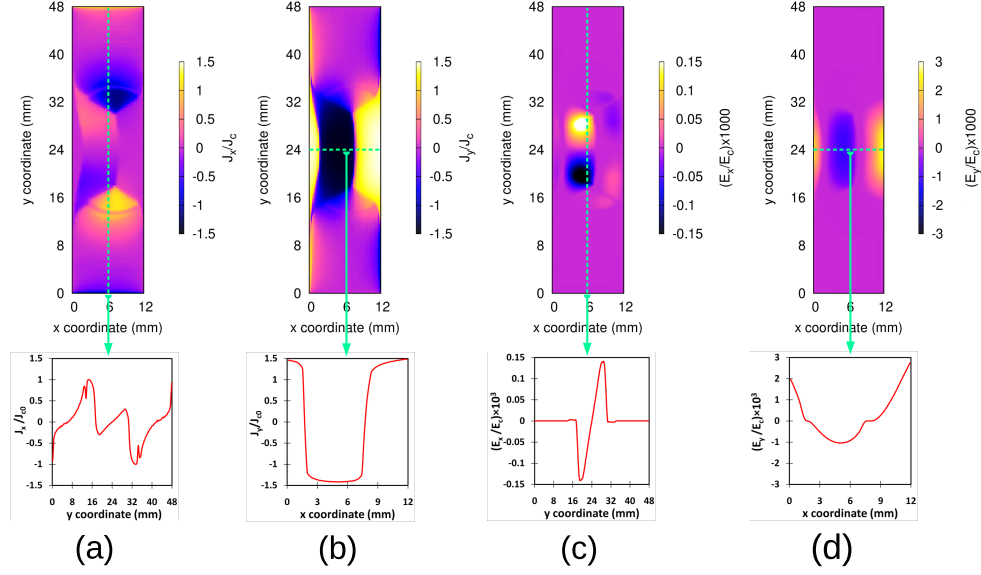


Figure 11: Modeling results for the x and y components of current density and electric field while the magnet is just on the top and concentric to the tape (step C in Figures 9 and 10) for airgap 3.3 mm and constant J_c . (a) J_c -normalized current map and current profile of J_x along the y axis in the middle of the tape (dashed green line), (b) J_c -normalized current map and current profile of J_y along the x axis in the middle of the tape (dashed green line), (c) E_c -normalized electric field map and electric field profile of E_x along the y axis in the middle of the tape (dashed green line), (d) E_c -normalized electric field map and electric field profile of E_y along the x axis in the middle of the tape (dashed green line).

For voltage signal measurements, the voltage taps should be placed in any area of the tape outside the two sides of the rectangle in order to measure the voltage signal accurately.

As a conclusion, the ratio of Tap Distance (TD) to Magnet Diameter (MD) (TD/MD) increased almost linearly with the airgap. Therefore, we can use the following relation for rough estimation of tab distance in the flux pump:

$$TD = (0.2AG + 1.3)MD, \quad (28)$$

where AG is the airgap distance.

6.3. Comparison to Experiments

In this section, we compare our 3D modeling results for the dynamo-type HTS flux pump with experiments published in [1] and with 2D MEMEP method presented in [9]. The calculations have been conducted with $J_c(B, \theta)$ dependence and with frequency of 12.3 Hz to be comparable with experimental results.

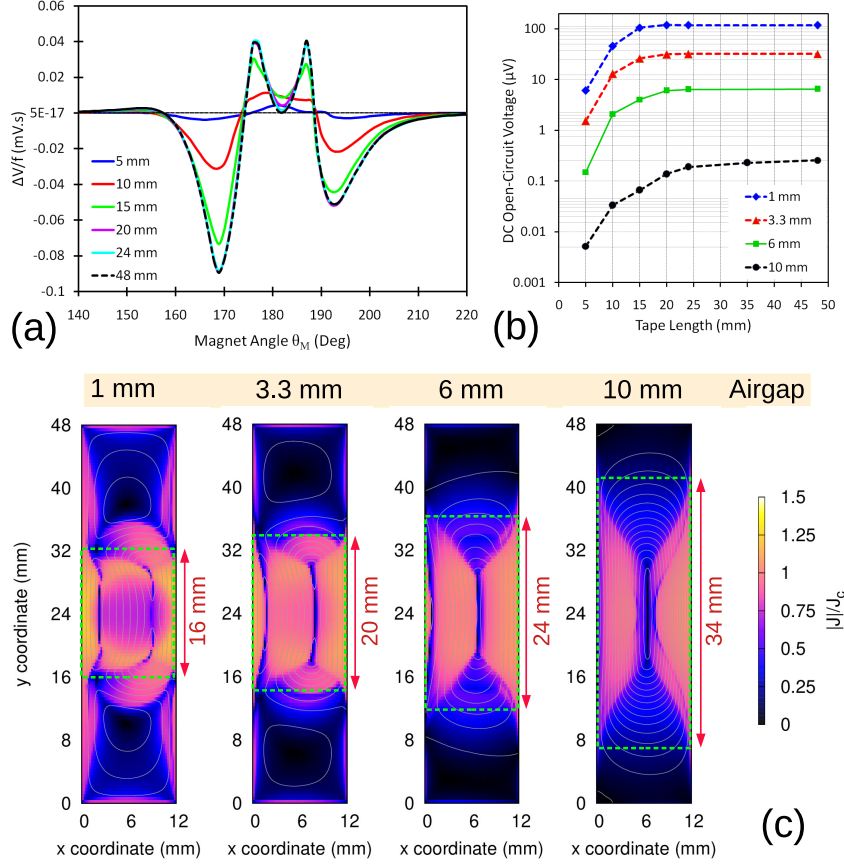


Figure 12: (a) Frequency-normalized ΔV (Equation (25)) against magnet angle θ_M for different tape lengths for airgap of 3.3 mm, (b) The DC open-circuit voltage value versus tape lengths for various airgaps, (c) Current modulus maps and current lines for different airgaps when the magnet is just in the middle and concentric to the tape ($\theta_M = 180^\circ$).

Figure 13 shows the results of the calculated and measured DC open-circuit voltage values for 5 different airgaps from 2.4 mm to 10.4 mm. Looking at the figure, it is obvious that the MEMEP 3D presents very good agreement with experiments and even better agreement than the MEMEP 2D method. In the case of MEMEP 2D, the decay of the DC voltage with the airgap is less pronounced than the measurements, with substantial differences at high airgaps. The reason is that the magnetic field of the magnet at 2D decays with the distance, r , as $1/r^2$ (infinitely long dipole), while for the real cylindrical magnet the magnetic field decays as $1/r^3$ (point dipole). This is the reason why 3D modeling agrees better with experiments. It is worth mentioning that, as discussed also in [9], the airgap measurement error is not negligible due to contraction and mechanical instability of the flux pump in liquid nitrogen bath (at least ± 0.5 mm airgap). This error is mostly noticeable in the lowest airgap of 2.4 mm, where a small difference in the airgap causes a high difference in the magnetic field from the magnet, and hence DC voltage. Should the gap be more accurately measured, we expect better

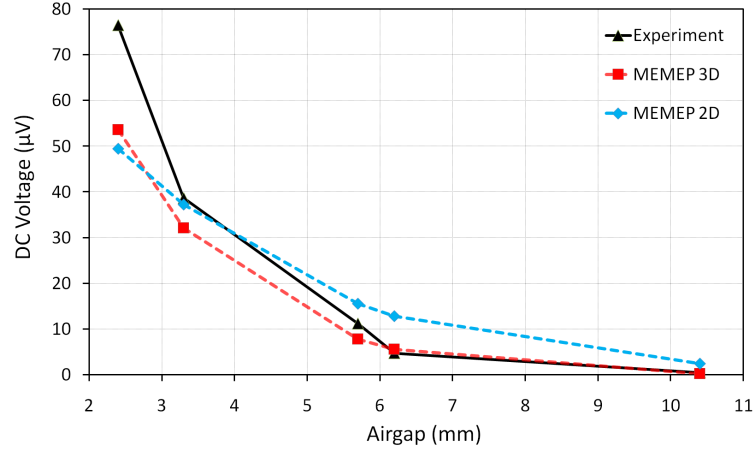


Figure 13: Comparison between DC open-circuit voltage values of different airgaps for calculated results of MEMEP 3D modeling against MEMEP 2D modeling presented in [9] and experiments conducted in [1]. Better agreement for 3D modeling is evident at large airgaps, while for low airgaps we expect significant measurement errors.

agreement between model and experiments at low gaps. Moreover, another source of discrepancy can be that the $J_c(B, \theta)$ in the model does not exactly correspond to that of the measurements, since the original tape is no longer available. As well, we needed to assume that $J_c(B, \theta, \phi) = J_c(B, \theta, \pi/2)$ for any ϕ because of unavailable measurements of this characteristics.

7. Conclusions

High-temperature superconducting (HTS) dynamos are promising devices that can inject large DC currents into the winding of superconducting machines or magnets in a contactless way. Thanks to this, troublesome brushes in HTS machines or bulky currents leads with high thermal losses will be no longer required. The working mechanism of HTS dynamo has been controversial during recent years and several explanations and models have been proposed to elucidate its performance.

In this thesis, we presented fast and accurate 2D and 3D modeling methods based on minimum electromagnetic entropy production (MEMEP) for analyzing the performance of a dynamo-type flux pump in open-circuit mode and charging a coil. In 2D and open-circuit mode, we focused on the effects of the airgap, the tape critical current density and the magnet geometry on the DC voltage generation in the HTS dynamo. To verify the modeling results, we compared them with measurements for several airgaps from [1]. For verification of our MEMEP 2D model in the coil charging case, we compared it with the segregated \mathbf{H} -formulation finite element method and analytical method, showing very good agreement. We presented also the first 3D model of a dynamo-type HTS flux pump based on MEMEP method. Employing the proposed model, the performance of the dynamo is investigated and analyzed in open-circuit mode.

Our presented MEMEP 2D model solves the Maxwell equations only inside the superconducting region with minimization of a functional. Thanks to this, it is efficient and fast, which provides the opportunity to model more complex geometries and parameter sweeps. The principle of flux pumps does not seem to be fully understood yet. Therefore, studying open-circuit mode, being more simple than full-circuit mode, is more helpful to understand its mechanism. By analyzing the DC open-circuit voltage in the airgap range between 2.4 to 50 mm, we found that the DC voltage generation does not cease even in large airgaps up to 50 mm, where the maximum perpendicular magnetic field density is only around 7 mT. The reason can be justified from the existence of overcritical regions near the tape edges even under small values of the magnetic field, which leads to the generation of DC voltage in the HTS tape. The comparison between modeling results with experimental studies obtained from [1] in the airgap range between 2.4 mm to 10.4 mm shows good agreement with experiments. We also found that the generated voltage in open-circuit for constant J_c does not depend on the J_c value, as long as the tape is fully saturated by screening currents and the magnetic field that they generate is much smaller than the magnet field. By changing the square magnet dimension, it is found that it is not necessary to have magnets narrower than the tape in order to achieve flux pumping. Also, the open-circuit voltage increases continuously with increasing the dimension of the magnet. This modeling method can open the way for fast and reliable studies in order to further analyze the behavior of flux pumps and to optimize their structures.

We benchmarked our MEMEP 2D method with nine other different numerical

methods to model an HTS dynamo in open-circuit mode and with constant J_c . These methods include **H**-formulation with shell current method, coupled **H-A** method, coupled **T-A** formulations, Segregated **H**-formulation, integral equation, and volume integral equation-based equivalent circuit method. All methods showed excellent quantitative and qualitative agreement with each other. The MEMEP 2D method was introduced as the clear winner in terms of computational speed.

The MEMEP 2D method was developed for describing the charging process of a coil by an HTS dynamo. This method was compared with the segregated **H**-formulation (SEG-H) and with an analytical method through nine different cases including three airgaps of 1, 2, and 3.7 mm and three frequencies of 4.25, 25, and 50 Hz. Firstly, the I - V curves of the modeled HTS dynamo and thus the effective resistances were calculated and compared together. The maximum percentage difference between the effective resistances of the two models was less than 2%, which occurred at the highest frequency and the smallest airgap. Then, the instantaneous voltage components and the dynamic charging current curve of the coil for the two models were calculated and compared together, which showed excellent quantitative and qualitative agreement. It was found that the current charging curve contains ripples within each cycle, which cannot be captured via the analytical method. Such ripples cause ripple AC loss in the flux pump itself and could also cause ripple AC loss in the coil being charged. The AC loss in the flux pump was shown to be almost constant during the whole charging process. Afterward, the charging process of a coil by the dynamo was investigated and there was again excellent quantitative and qualitative agreement between the two models and the analytical method. In all, the presented MEMEP method showed promising performance to describe the charging process of an HTS dynamo over thousands of cycles, as well as capturing the current ripple within a cycle. In addition, the flexibility of the MEMEP 2D modeling framework presented here has the potential to be coupled with other multiphysics analyses, as well as with a MEMEP model of an HTS coil. Besides, the model is capable of studying HTS dynamos with nonlinear I - V characteristics and their influence on the dynamics of the charging process.

In addition, the first 3D model of an HTS flux pump has been presented and verified against the experiment. This model can help to clarify the complicated mechanism of HTS dynamo-type flux pumps and verify the previously proposed mechanism by 2D models. The unique features of the presented 3D model, based on MEMEP enable to perform computations in conveniently short times makes the model very fast and efficient (solving the Maxwell equations only inside the superconductor, fast solver by division into sectors and iteration, and use of parallel computing). As found for cross-sectional 2D methods [13], MEMEP 3D could likely be faster than conventional commercial finite-element methods, since it avoids the problem of rotating mesh in the air. However, a fair comparison will require a dedicated benchmark with several methods. Employing MEMEP 3D, we studied the screening current distribution, which in its overcritical form is the reason for

flux pumping phenomenon, across the tape surface and in several key positions of the magnet movement. We investigate the role of the x and y components of the electric field and screening current in generating the voltage in the flux pump. It was found that, while the magnet traverses the tape, the maximum value of the y component of the electric field, E_y , is around 20 times larger than E_x , which highlights the role of J_y to generate the voltage throughout the tape surface. In addition, the average E_x across the sample vanishes because of symmetry. We also studied the effect of the tape length on voltage generation in the flux pump. We found that the distance between voltage taps for precise measuring of the voltage depends on not only the diameter of the magnet but also the distance between the magnet and the tape surface. The ratio of tap distance to magnet diameter increased almost linearly with the airgap. We expect that the minimum tape length will keep increasing with the separation. Finally, the calculated modeling results were compared against experiments for several airgaps, which showed very good agreement.

In summary, the contributions of this thesis are as follows:

- We presented a fast 2D model based on minimum electromagnetic entropy production (MEMEP) for analyzing the performance of a dynamo-type flux pump in open-circuit mode with good agreement with measurements.
- We benchmarked our MEMEP 2D method with nine other different numerical methods to model an HTS dynamo in open-circuit mode. All methods showed excellent quantitative and qualitative agreement with each other and our MEMEP 2D method was recognized as the fastest method in terms of computational speed.
- We developed the MEMEP 2D method for describing the charging process of a coil by an HTS dynamo and we cross-checked the validity of the results with the segregated \mathbf{H} -formulation finite element method (calculated in University of Cambridge) and analytical method showing very good agreement.
- We presented the first 3D model of an HTS flux pump with good agreement against the experiment. Our 3D model is very fast and efficient due to solving the Maxwell equations only inside the superconductor region, division into sectors and iteration, and use of parallel computing.
- Thanks to our 3D model and for the first time, we studied the screening current distribution, which in its overcritical form is the reason for flux pumping phenomenon, across the tape surface in several key positions of the magnet movement.

Publications and Conferences

Publications

- **Asef Ghabeli**, E. Pardo, and M. Kapolka, “3D modeling of a superconducting dynamo-type flux pump”, *Scientific Reports*, vol. 11, no. 1, 10296, May 2021.
DOI: <https://doi.org/10.1038/s41598-021-89596-4>
- **Asef Ghabeli** and E. Pardo, “Modeling of airgap influence on DC voltage generation in a dynamo-type flux pump”, *Superconductor Science and Technology*, vol. 33, no. 3, p. 035008, feb 2020.
DOI: <https://doi.org/10.1088/1361-6668/ab6958>
- **Asef Ghabeli**, M. Ainslie, E. Pardo, L. Quéval and R. Mataira “Modeling the charging process of a coil by an HTS dynamo-type flux pump”, Preprint.
DOI: <http://arxiv.org/abs/2105.00510>.
- M. Ainslie, F. Grilli, L. Quéval, E. Pardo, F. Perez-Mendez, R. Mataira, A. Morandi, **Asef Ghabeli**, C. Bumby, and R. Brambilla,
”A new benchmark problem for electromagnetic modelling of superconductors: the high- T_c superconducting dynamo.” *Superconductor Science and Technology*, vol. 33, no. 10, p. 105009, sep 2020.
DOI: <https://doi.org/10.1088/1361-6668/abae04>
“Corrigendum: A new benchmark problem for electromagnetic modelling of superconductors: the high- T_c superconducting dynamo (2020 supercond. sci. technol. 33105009),” *Superconductor Science and Technology*, vol. 34, no. 2, p.029502, jan 2021.
DOI: <https://doi.org/10.1088/1361-6668/abd522>
- F. Gomory, J. Souc, M. Adamek, **Asef Ghabeli**, M. Solovyov, and M. Vojenciak.
”Impact of critical current fluctuations on the performance of a coated conductor tape.” *Superconductor Science and Technology*, vol. 32, no. 12, p. 124001, 2019.
DOI: <https://doi.org/10.1088/1361-6668/ab4638>.
- M. Buran, M. Vojenciak, M. Mosat, **Asef Ghabeli**, M. Solovyov, M. Pekarcikova, L. Kopera, and F. Gomory. ”Impact of REBCO coated conductor stabilization layer on the fault current limiting functionality.” *Superconductor Science and Technology*, vol. 32, no. 9, p. 095008, 2019.
DOI: <https://doi.org/10.1088/1361-6668/ab2c8e>.

Conference Presentations

- **Asef Ghabeli**, E. Pardo, M. Kapolka
Invited Poster ”3D modeling of a superconducting dynamo-type flux pump”, Applied Superconductivity Conference 2020 (ASC 2020), Virtual Conference, 23 October- 7 November 2020,

<https://doi.org/10.5281/zenodo.4264833>.

- **Asef Ghabeli**, E. Pardo, M. Soloviov, J. Souc
Invited Poster "Modeling and measurement of the voltage signal in HTS flux pumps", EUCAS Conference, 1st-5th September 2019, Glasgow, Scotland,
<https://doi.org/10.5281/zenodo.3547548>.
- **Asef Ghabeli**, E. Pardo, M. Kapolka
On-demand Presentation "3D Modeling of Screening Currents and Voltage in a Superconducting Flux Pump with Transport Current", 2021 Virtual MRS Spring Meeting & Exhibit.
- **Asef Ghabeli**, E. Pardo, M. Ainslie, L. Quéval
Poster "Modeling HTS dynamo-type flux pumps: open-circuit mode and charge of an HTS coil", 7th International Workshop on Numerical Modelling of High Temperature Superconductors, Virtual (Nancy, France), 22-23 June 2021.

References

- [1] C. W. Bumby, Z. Jiang, J. G. Storey, A. E. Pantoja, and R. A. Badcock, “Anomalous open-circuit voltage from a high- T_c superconducting dynamo,” *Applied Physics Letters*, vol. 108, no. 12, p. 122601, 2016.
- [2] E. Pardo, J. Šouc, and L. Frolek, “Electromagnetic modelling of superconductors with a smooth current–voltage relation: variational principle and coils from a few turns to large magnets,” *Superconductor Science and Technology*, vol. 28, no. 4, p. 044003, 2015.
- [3] E. Pardo and M. Kapolka, “3D computation of non-linear eddy currents: Variational method and superconducting cubic bulk,” *Journal of Computational Physics*, vol. 344, pp. 339–363, 2017.
- [4] F. Grilli, E. Pardo, A. Stenvall, D. N. Nguyen, W. Yuan, and F. Gmry, “Computation of losses in HTS under the action of varying magnetic fields and currents,” *IEEE Transactions on Applied Superconductivity*, vol. 24, no. 1, pp. 78–110, 2014.
- [5] S. Li, J. Kováč, and E. Pardo, “Coupling loss at the end connections of REBCO stacks: 2D modelling and measurement,” *Supercond. Sci. Technol.*, vol. 33, no. 7, p. 075014, 2020.
- [6] R. Mataira, M. Ainslie, A. Pantoja, R. Badcock, and C. Bumby, “Mechanism of the high- T_c superconducting dynamo: Models and experiment,” *Phys. Rev. Applied*, vol. 14, p. 024012, 2020.
- [7] R. Mataira, M. D. Ainslie, R. Badcock, and C. W. Bumby, “Modeling of stator versus magnet width effects in high- T_c superconducting dynamos,” *IEEE Transactions on Applied Superconductivity*, vol. 30, no. 4, pp. 1–6, 2020.
- [8] Z. Jiang, K. Hamilton, N. Amemiya, R. A. Badcock, and C. W. Bumby, “Dynamic resistance of a high- T_c superconducting flux pump,” *Applied Physics Letters*, vol. 105, no. 11, p. 112601, 2014.
- [9] A. Ghabeli and E. Pardo, “Modeling of airgap influence on DC voltage generation in a dynamo-type flux pump,” *Superconductor Science and Technology*, vol. 33, no. 3, p. 035008, 2020.
- [10] R. C. Mataira, M. D. Ainslie, R. A. Badcock, and C. W. Bumby, “Origin of the DC output voltage from a high- T_c superconducting dynamo,” *Applied Physics Letters*, vol. 114, no. 16, p. 162601, 2019.
- [11] Z. Jiang, C. W. Bumby, R. A. Badcock, H. Sung, N. J. Long, and N. Amemiya, “Impact of flux gap upon dynamic resistance of a rotating HTS flux pump,” *Superconductor Science and Technology*, vol. 28, no. 11, p. 115008, 2015.
- [12] L. Quéval, K. Liu, W. Yang, V. M. Zermeño, and G. Ma, “Superconducting magnetic bearings simulation using an H-formulation finite element model,” *Superconductor Science and Technology*, vol. 31, no. 8, p. 084001, 2018.
- [13] M. D. Ainslie, F. Grilli, L. Quéval, E. Pardo, F. Perez-Mendez, R. Mataira, A. Morandi, A. Ghabeli, C. Bumby, and R. Brambilla, “A new benchmark problem for electromagnetic modelling of superconductors: the high- T_c superconducting dynamo,” *Superconductor Science and Technology*, vol. 33, no. 10, p. 105009, 2020.